Materials Physics and Mechanics 44 (2020) 271-287 Received: July 7, 2019

EVALUATION OF DAMAGE INDUCED IN GRAPHITE DUE TO SAMPLE PREPARATION BY STANDARD NON-DESTRUCTIVE TECHNIQUES

Michael Lasithiotakis[1*], James T. Marrow[2], Barry J. Marsden[3]

[1]Greek Atomic Energy Commission, P.O BOX 60092, P.C. 15341, Agia Paraskevi – Athens, Greece

[2]Department of Materials, University of Oxford, Parks Road, Oxford OX1 3PH, UK

[3]Nuclear Graphite Research Group, School of Mechanical, Aerospace and Civil Engineering, The University of Manchester, Manchester M13 9PL, UK

*e-mail: michalis.lasithiotakis@eeae.gr

Abstract. Damage introduced to graphite by mechanical polishing, argon ion beam polishing, fracture, and neutron bombardment has been studied in polycrystalline graphites and Highly Oriented Pyrolytic Graphite (HOPG). Scanning Electron Microscopy and Atomic Force Microscopy, as well as X-Ray Diffraction and Raman spectroscopy, were employed. The least disturbed surfaces are observed in pristine HOPG or by fracturing techniques that exposed pre-existing defects. A decrease of the mean particle size of the abrading medium and the use of ions and neutrons increased the D band and decreased the pseudo–crystallinity.
Keywords: graphite, ion irradiation, surface preparation

1. Introduction

As well as its use as a neutron moderator, graphite also acts as a structural material in some designs of nuclear reactor fuels. Graphite bombardment with particles such as ions and neutrons create defects [1-5], and the fast neutron bombardment causes significant property changes in graphite that take place as the reactor ages, such as dimensional changes and creep and changes to physical properties, including Young's modulus, strength, coefficient of thermal expansion and thermal conductivity [6-12]. To gain an understanding of the property/structure relationships in graphite, non-destructive characterization techniques such as scanning electron microscopy (SEM) and transmission electron microscopy (TEM) [13] have been extensively used. It is important that for these non-destructive methods, and graphite, sample preparation does not introduce significant microstructural damage. Sample preparation methods should induce as few artefacts as possible [14]. This issue has been deeply addressed in metals (e.g. [15]), but there is less knowledge of sample preparation effects in graphite, for which the sample preparation techniques for microscopy have been mainly based on mechanical polishing, such as tripod polishing [16] or ion beam polishing techniques [17,18].

In this work, a range of surface preparation techniques has been evaluated for graphite. The methods that were examined include standard metallographic techniques and additionally fracture to produce a surface that was as undisturbed as possible. Neutron irradiated poly-granular graphite extracted from a nuclear reactor core (British Experimental Pile Zero, BEPO) and undamaged graphite (Highly Oriented Pyrolytic Graphite, HOPG) serve as abstract examples of damaged and undisturbed structures respectively. Highly Oriented

http://dx.doi.org/10.18720/MPM.4432020_1
© 2020, Peter the Great St. Petersburg Polytechnic University
© 2020, Institute of Problems of Mechanical Engineering RAS

Pyrolytic Graphite (HOPG) is commonly used as a model material for graphitic single crystals [19-22]. They are used as a reference against which to evaluate the mechanical and ion damage introduced to polygranular Gilsocarbon graphite, which is the polycrystalline artificial graphite specifically manufactured for the UK Advanced Gas Reactors [23-25]. The specimens are examined using standard non-destructive surface characterization techniques of Atomic Force Microscopy, Optical, and Scanning Electron Microscopy, as well as spectroscopic methods, such as X-Ray Diffraction and Raman spectroscopy.

2. Methods

Gilsocarbon Polycrystalline Graphite Preparation: Mechanical Polishing and Fracturing. Gilsocarbon polycrystalline graphite surfaces were prepared by simple manual polishing on a metallographic grinding wheel, operated at 200 rpm with tap water as a coolant. During grinding, no additional pressure was applied other than the sample's own weight. The grinding time was three minutes using coarse silicon carbide grinding paper (P800 – 21.8 μm), and then three additional minutes using a finer grade of silicon carbide grinding paper (P4000 – 5 μm). Polishing, also with no additional pressure, took place for three minutes on felt, smeared with diamond paste (Preparationes Diamantee Mecaprex) of nominal mean grain size of 3 μm, and then three more minutes with 1 μm diamond paste at 200 rpm. Diamond paste acted as a polishing agent and as a lubricant. After every polishing stage, the specimens were washed with ethanol and air dried.

A fractured surface was obtained by dropping a 1 kg stainless steel wedge from a height of 1 meter onto the center of a perpendicularly arrange piece of graphite measuring 3 cm × 3 cm × 10 cm. Graphite dust was obtained by dropping a cylindrical stainless steel bar (3 cm diameter by 4.5 cm height) from a height of 1 meter onto a particle of graphite of a few millimeters in diameter, placed on top of a stainless steel plate.

Highly Oriented Pyrolytic Graphite (HOPG) Preparation. A specimen of Highly Oriented Pyrolytic Graphite (HOPG) [26,27] produced by SPI Supplies U.S.A and measuring approximately 1 cm × 1 cm × 0.1 cm, was cold mounted in resin and cut into pieces of 3 mm × 3 mm × 1 mm approximately. The resin was removed and each specimen was then cut to dimensions of 3 × 3 mm and thickness of less than 0.5 mm. The large surfaces were then cleaned by stripping with adhesive tape until a clear "mirror" surface was produced.

BEPO Graphite - Occurrence, Sampling, and Preparation. Samples of neutron irradiated polycrystalline graphite from British Experimental Pile Zero (BEPO) were obtained from the United Kingdom Atomic Energy Authority (UKAEA), with permission from the UK Nuclear Decommissioning Authority (NDA). The sample had been removed from a four-inch diameter cylinder (section 20, Fig. 1), which was part of a core bored through the reactor bio-shield and reactor core in 1975 [28]. This section had received a fast neutron fluence of 11.3×1020 n/cm2 EDND (Equivalent DIDO Nickel Dose) at an estimated irradiation temperature of between 100 and 120°C [30]. The BEPO graphite core was annealed several times in its lifetime in order to remove stored energy [30], and this may have affected the irradiation damage. The specimen was stored inside the active laboratory of SERCO Ltd. (now Wood PLC) where twenty samples were machined into small cylindrical disks, inside a radiation proof glove box. A Secotom Diamond Cutting machine, operating at 2500 rpm, was used to cut 6 mm diameter cylinders into disks approximately 1.5 mm thick. The mean sample weight was ~70 mg. Some of the cylindrical disks were fractured to create fresh surfaces for observation and characterization. The fracturing of BEPO cylinders took place by placing the disks between two pieces of steel. The upper steel part had a wedge shape and the lower part had a V shaped groove, into which the wedge could fit precisely. The graphite discs were placed horizontally inside the groove and the wedge was placed over of the discs. The discs were then fractured in two halves by a blow delivered by a hammer to the wedge.

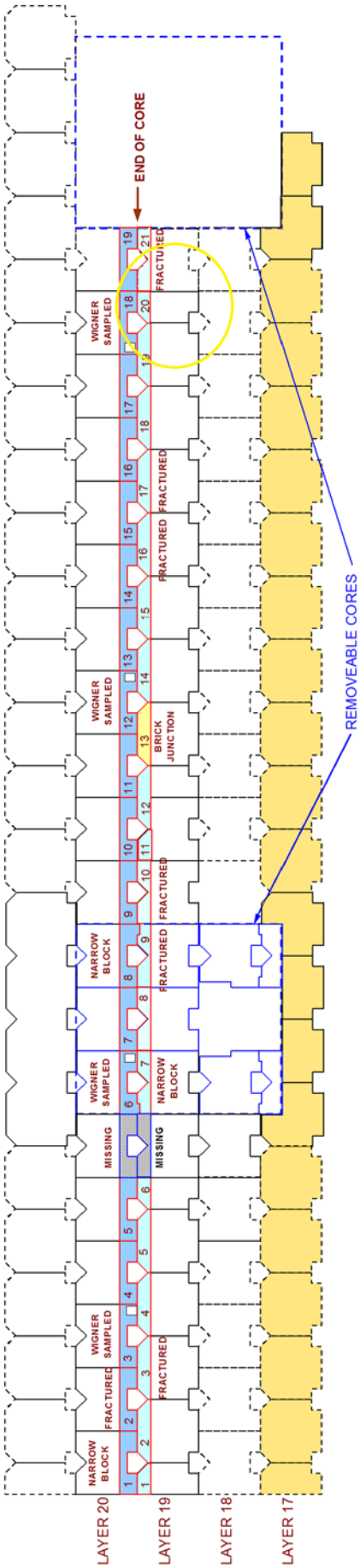

Fig. 1. The 4-in. core section is taken from BEPO as depicted in the diagram. Samples were obtained from section 20 at the end of core (in yellow circle). All the examined specimens in this work came from the lower section of the core, which is shaded (light blue) [29]

Ion Beam Irradiation – Method. Ion beam polishing of Gilsocarbon and HOPG specimens was achieved using a precision ion polishing system (Gatan – PIPS), which is designed to prepare specimens for TEM. Two argon beams from opposing directions with a maximum energy of irradiation of 6 keV were used. This energy was used with an angle of irradiation of 5°, which gave the maximum ion beam current. A vacuum was maintained in the irradiation polishing chamber (~10-5 torr) throughout the irradiations. Five samples each of Gilsocarbon and HOPG were polished thus for four hours each. The argon ion beam intensity followed a sinusoidal variation of a five seconds period, between 4 and 30 mA.

Simulation of atomic displacement induced by ion bombardment. Atomic displacements and subsequent cascades, caused by ion polishing in HOPG and Gilsocarbon were calculated using the TRIM code [31]. The trajectories of the argon ions within the mass of Gilsocarbon and HOPG are visualized based on the assumption that the ions are bombarding the graphitic surfaces at one point. No alteration of the physical surface, such as abrasion, or ablation, by the ion beam has been assumed (Fig. 2).

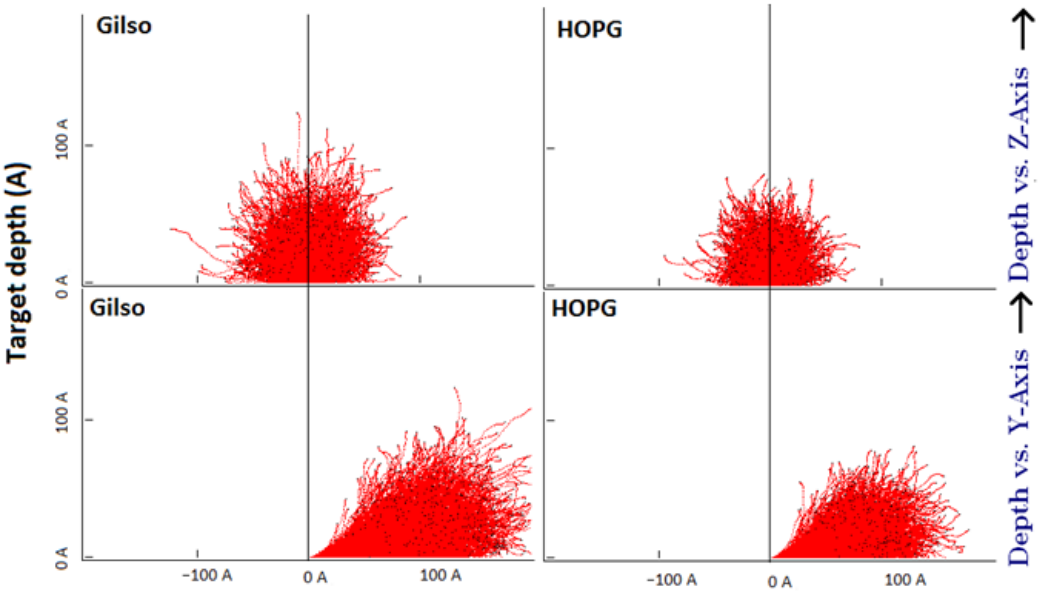

Fig. 2. Calculation of the penetration depth for argon ions for HOPG and Gilsocarbon. Trajectories of the ions (in red) parallel to the irradiation point (at the center of x axis)

Mean penetration depths of less than 80-90 nm for HOPG and less than 120-130 nm for Gilsocarbon were calculated by the model, due to the difference in density between the two graphite types. The irradiation polishing damage intensity drops to less than 5% of the mean at a distance of 50-60 nm from the surface for HOPG and 70-80 nm for Gilsocarbon.

3. Results

Microscopic Investigation of Damage. Optical microscopy observations are summarised in Fig. 3. This shows that qualitatively at the length scale of a few 10's of μm, the smoothest surfaces are achieved in HOPG by cleaving with adhesive tapes (Fig. 3, b1). They were followed by selected regions of the fractured Gilsocarbon surfaces (Fig. 3, a1, a7) and Gilsocarbon surfaces produced by ion beam irradiation (Fig. 3, a6). Mechanical polishing with P4000 of Gilsocarbon (Fig. 3, a3) followed. Diamond paste (Fig. 3, a4, a5) produced rougher surfaces than P4000. On HOPG (Fig. 3, b1 and b2), ion beam irradiation disrupted

the original "mirror" surface and produced formations resembling fish scales. The BEPO graphite surfaces (Fig. 3, c1) were similar to fractured Gilsocarbon (Fig. 3, a1, a7).

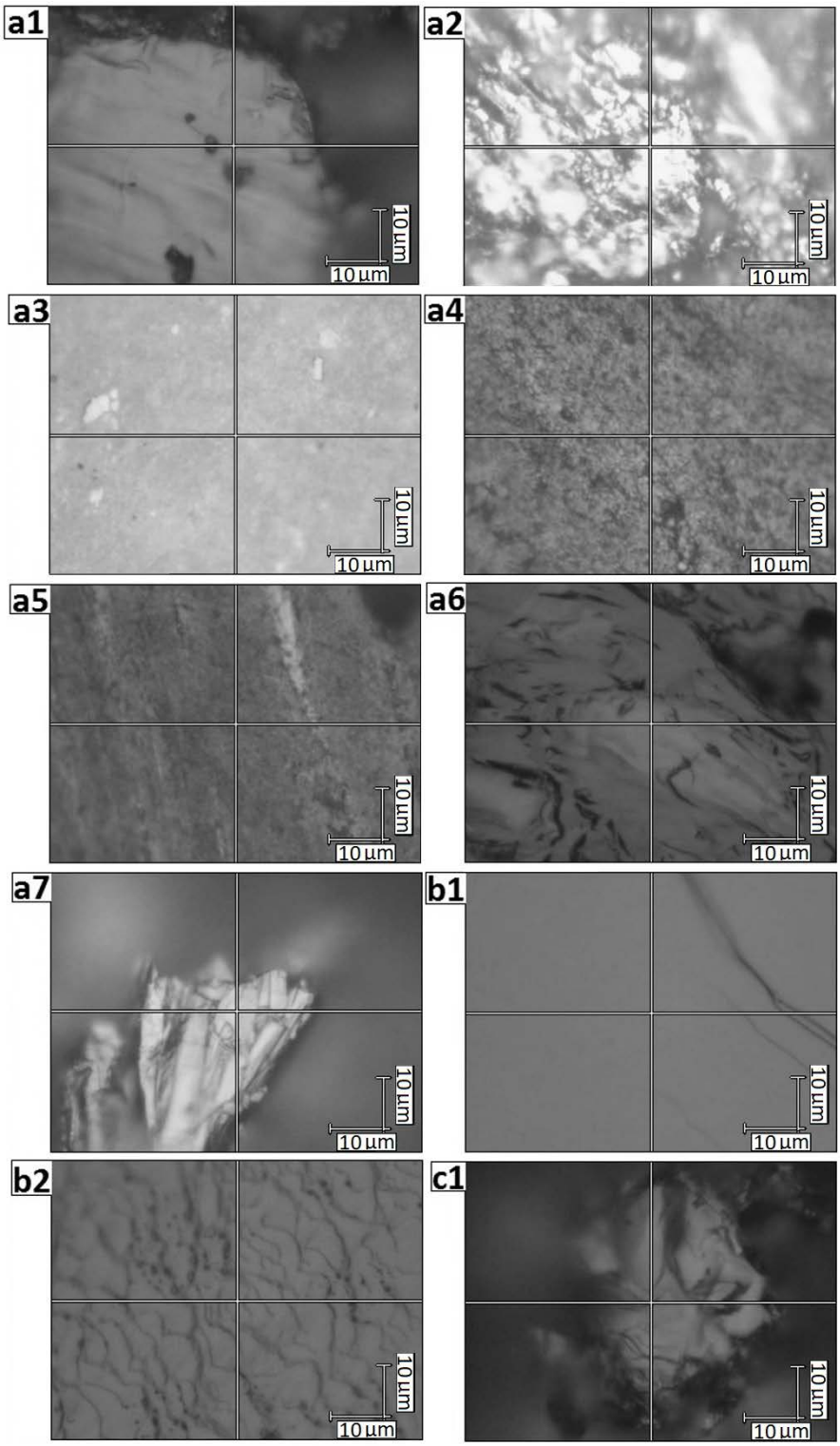

Fig. 3. Optical micrographs of a1 – Gilsocarbon fractured, a2 – Gilsocarbon polished with P800, a3 – Gilsocarbon polished with P4000, a4 – Gilsocarbon polished with diamond paste of 3µm, a5 – Gilsocarbon polished with diamond paste of 1µm, a6 – Gilsocarbon ion beam milled with 6keV argon ion beams, a7 – Gilsocarbon dust particle produced by fracturing, b1 – HOPG non irradiated, freshly cleaved, b2 – HOPG ion beam milled with 6keV argon ion beams, c1 – BEPO neutron irradiated and fractured

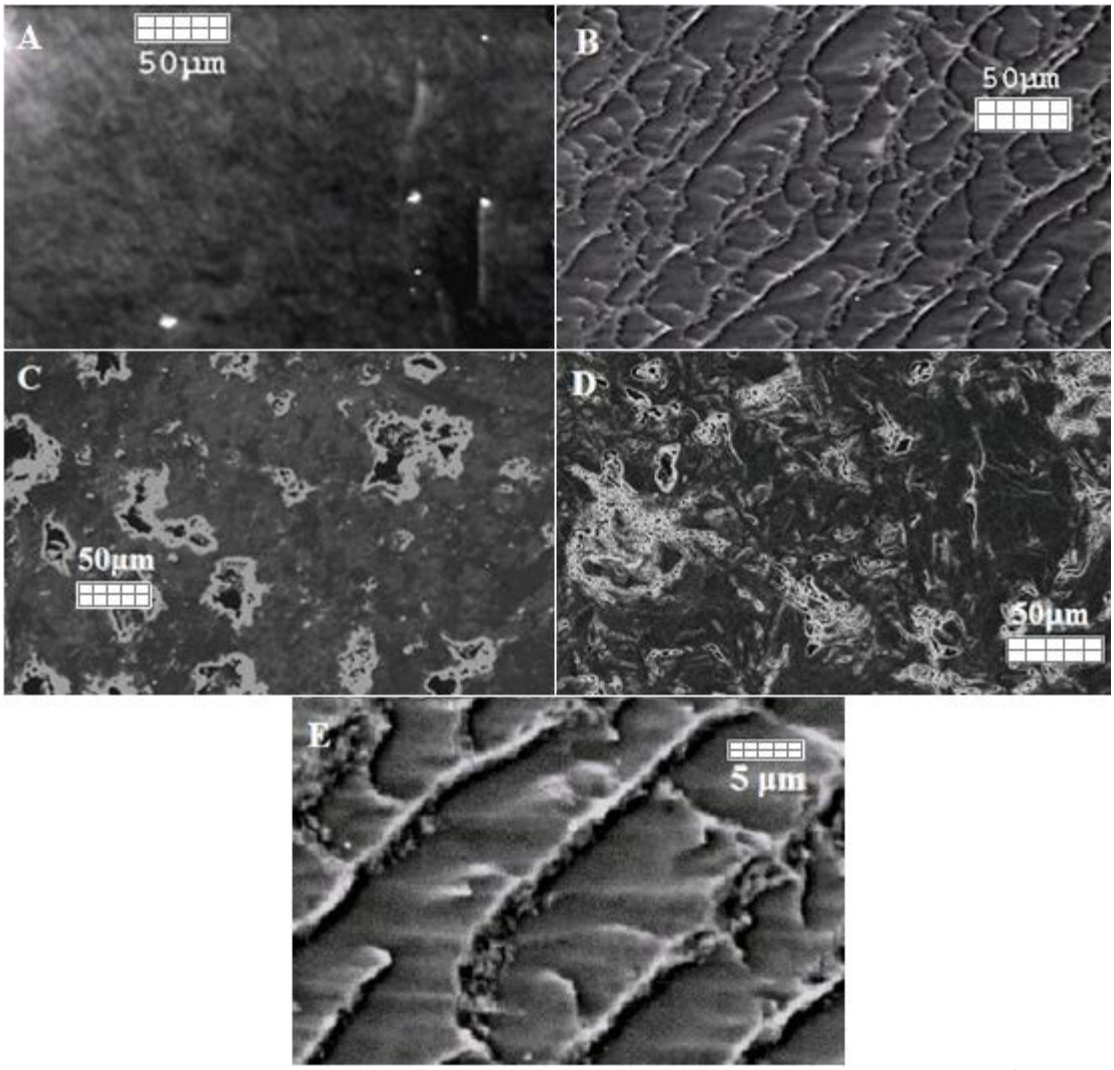

Fig. 4. Non irradiated, freshly cleaved HOPG (A), Irradiated HOPG with Ar^+ of 6keV ion beam (B), Mechanically polished Gilsocarbon with P4000 (C), Irradiated Gilsocarbon with Ar^+ of 6keV ion beam (D), Corrugations and trenches appear after irradiation of HOPG(E)

Scanning electron microscopy images (secondary electrons) of ion polished polycrystalline Gilsocarbon and HOPG, and mechanically polished Gilsocarbon, were obtained in an AmRay 1810 Scanning Electron Microscope at 10kV accelerating voltage. (Fig. 4). As found in the optical observations, the HOPG (Fig. 4 b) has corrugations that are absent on pristine HOPG (Fig. 4 A). The ion irradiated Gilsocarbon (Fig. 4, c, d) surfaces show an increase in fine porosity compared with the non-irradiated samples.

The effects of ion irradiation on topography were also examined by Atomic Force Microscopy (AFM), using a VEECO MultiMode V atomic force microscope under tapping mode. AFM was attempted on all samples except the fractured ones, as these had macroscopic roughness that prevented AFM observation. Most of the other samples were too rough to produce good quality images, but data were obtained for HOPG Non-Irradiated, Irradiated, Gilsocarbon, and Polished P4000 (Fig. 5).

Topography and phase of oscillation maps and values (Table 1) were obtained. In HOPG these reveal finer scale features (Fig. 5 a and b) that were not observable by SEM.

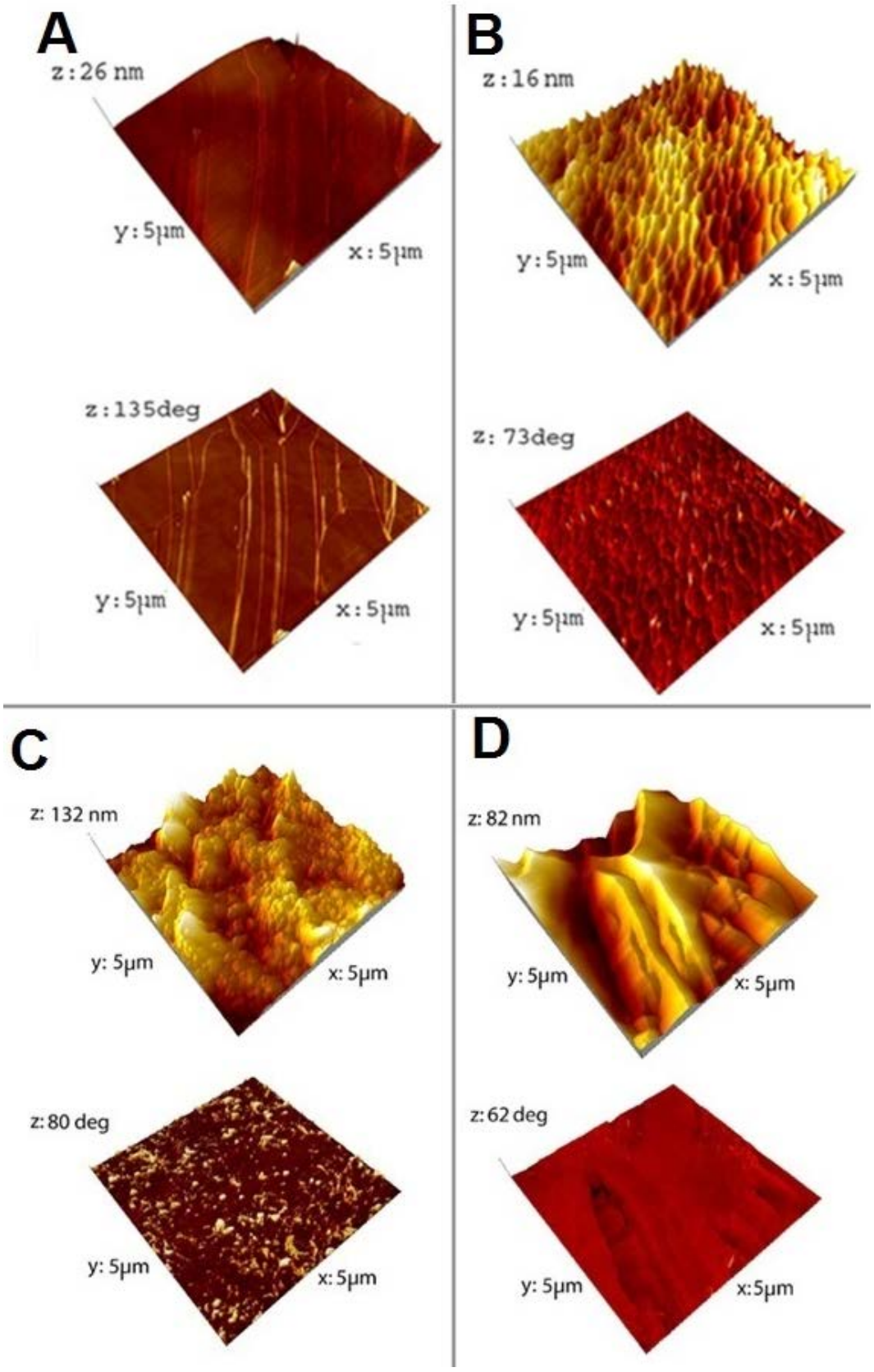

Fig. 5. Atomic Force Microscopy images for HOPG before (A) and after (B) irradiation, and mechanically polished Gilsocarbon by P4000 (C) and the same specimen after ion irradiation (D). The figure shows the topography (top), and phase of oscillation (bottom) before and after irradiation for all samples mentioned

Table 1. Statistical parameters analysis for the maps of height and phase of the oscillation, produced for HOPG and Gilsocarbon (1 μm polish) before and after irradiation by Ar^+ ion milling

		HOPG Non Irradiated	HOPG Irradiated	Gilso-carbon P4000	Gilso- carbon Irradiated
Roughness Average	(nm)	0.83	2.39	14.2	11.9
Root Mean Square	(nm)	1.04	2.99	18.30	14.70
Surface Skewness	-	-0.397	-0.0137	0.275	-0.0366
Surface Kurtosis	-	3.66	2.92	3.59	2.65
Surface Area Ratio	-	0.01520	0.07210	1.26000	0.22800

The obtained statistical parameters were the roughness average, surface skewness, and kurtosis, and surface area ratio [32-35]. The surface skewness describes the asymmetry of the height distribution histogram, and the surface area ratio expresses the ratio between the surface area (taking the z height into account) and the area of the projected xy plane. The surface area ratio expresses the ratio between the surface area (taking the z height into account) and the area of the flat xy plane. The data are summarized in Table 1. HOPG, with irradiation, shows an increase of surface roughness, which is consistent with the observed corrugations of most of the basal flat surfaces (Fig. 2). In contrast, ion beam milling leads to a decrease in surface roughness in Gilsocarbon. Hence the surface area ratio increases for HOPG and decreases for Gilsocarbon.

X-Ray Diffraction (XRD). Measurements of lattice parameters by the standard non-destructive XRD technique in graphite[36,37] have shown that irradiation induced damage in graphitic materials increases the interlayer spacing, i.e. d(002), as the degree of crystallinity decreases[38,39]. It has been suggested that the lattice parameter changes are linear with fluency, up to 3×1018ncm−2 EDND [40]. The apparent crystallite size can be obtained from peak broadening, and this also changes with irradiation. For instance, Wang et al. measured crystallite sizes of various types of graphite in the range of 300-400Å using the (002) and (110) Bragg peaks [41] and XRD studies of highly irradiated graphite, by Kelly et al. [41] exhibited broad and asymmetric peaks suggesting a decrease in crystallinity. Lexa et al. [42] obtained simultaneous XRD measurements in combination with Differential Scanning Calorimetry measurements to examine the annihilation of neutron irradiation induced damage in graphite, and quantified diffraction peak broadening by measuring the full width half maximum (FWHM) of the (002) peak. This is inversely proportional to the dimensions of the crystallite L and can be represented by the Scherrer equation [43] to give:

$$\mathrm{FWHM} = \frac{K\lambda}{L\cos\theta}, \quad (1)$$

where K is an empirical dimensionless constant referred as the crystalline shape factor (0.89), λ is the X-ray wavelength, L is the crystalline diameter in Angstroms and θ is the Bragg angle at peak maximum. For (002) diffraction peaks, the graphite crystallite dimension is commonly referred to as Lc.

XRD measurements were made on samples of neutron irradiated BEPO graphite, Gilsocarbon polished with 1μm diamond paste (initial XRD measurements showed no

differences in spectra between all the mechanically polished Gilsocarbon samples), ion irradiated Gilsocarbon (initially 1 μm polish), non-irradiated freshly cleaved and stripped HOPG and ion irradiated HOPG. A Philips X'Pert MPD θ/2θ X-ray diffractometer was used (CuKa, λ = 1.542 Å) to scan the range between 5-95° 2θ at a rate of 0.75°/min.

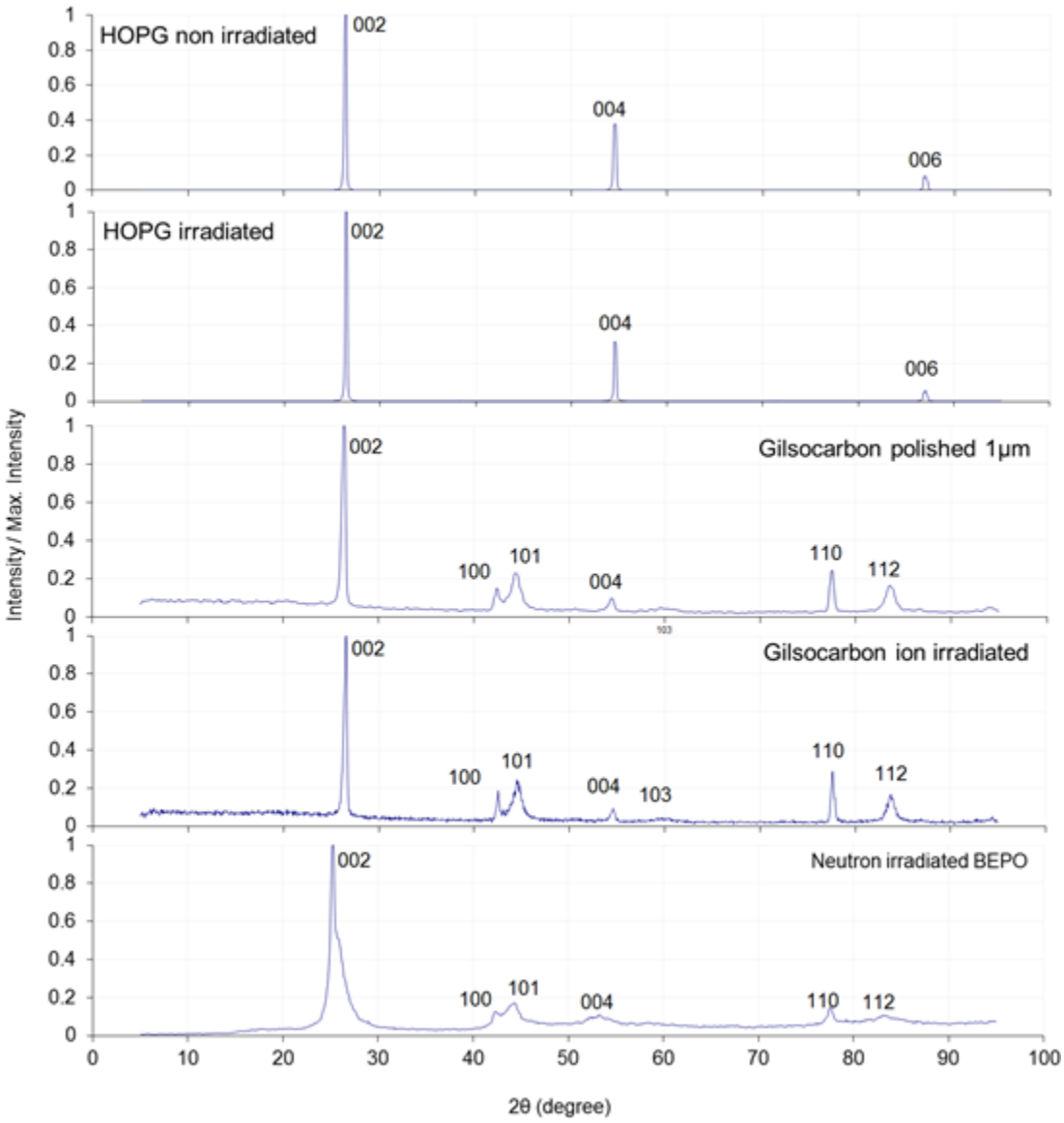

Fig. 6. HOPG non irradiated, and HOPG irradiated, Gilsocarbon polished with the diamond paste of -1μm, ion irradiated, and neutron irradiated BEPO graphite (CuKa, λ = 1.542 Å)

The spectra derived (Fig. 6) for HOPG show no distinctive differences in the characteristic peaks with ion irradiation. The neutron irradiated BEPO samples show evident broadening of the (002) peak and greater broadening of the (100) and (101) peaks at 42°, 44° and particularly the (112) peak at 83°. The (002) peak position was used to calculate the basal plane lattice *c*-spacing (Table 2), which for non-irradiated HOPG and Gilsocarbon was between 6.72 and 6.76 Å, in accordance with other studies [44].

Table 2. Data for c-spacing and mean crystalline size of specimens (variation of less than 5%)

	Polishing Particle Size	d(002)=c/2 (Angstroms)	Crystalline Size (Angstroms)
Gilso Polished P800	21.8 μm	3.37	294.11
Gilso Polished P4000	5 μm	3.36	292.85
Gilso Polished 3μm	3μm	3.37	293.79
Gilso Polished 1μm	1μm	3.39	293.68
Gilso Ion Polished	-	3.36	241.15
BEPO Neutron Irradiated	-	3.54	78.60
HOPG Ion Polished	-	3.38	293.68
HOPG Pristine	-	3.38	288.43
Gilso Dust	-	3.38	295.17
Gilso Fractured	-	3.35	291.45

The BEPO graphite c-spacing is around 7 Å, which is equivalent to a change of 4.7% in $\Delta c/c$, and is of the same order of the 25% increase reported for a fluence of 16.2×10^{20} n/cm^2 EDND [45]. This suggests that the estimated BEPO dose of 11.3×10^{20} n/cm^2 EDND is reasonable. The mean crystalline sizes along the *c*-direction, calculated using equation (8), are 288 to 293 Å for all graphite grades except the ion irradiated Gilsocarbon (241 Å).

Raman Spectroscopy. The basic peaks of a Raman spectrum of a graphitic material [46-48] are a first order peak at 1580 cm^{-1}, attributed to the ordered Raman-active peak and designated the G mode (after the space symmetry E2g), and three other first-order peaks approximately at 1340-1346cm^{-1}(D_1),1367cm^{-1} (D_2) and 1622cm^{-1} (D_0). Second-order peaks may be observed at 2680 ($2D_1$), 2730 ($2D_2$), 3250 ($2D_0$) cm^{-1}. The D peaks originate from disordered graphitic structures. The D_1 peak around 1340 cm^{-1} is a breathing mode of A1g symmetry [49] that is forbidden in perfect graphite and only becomes active in the presence of disordered graphite as disorder destroys the sp2 standard graphitic structure [50]. It has been observed [51] that the intensity ratio of the D_1 to G peaks (the D_1/G ratio) for pristine HOPG increases after ion bombardment, and the D_1 mode was observed only [52] when the ion irradiation fluence reached a critical value; the critical value decreased when heavier ions were used in the bombardment. The D_1/G ratio is affected by the charge state of the colliding particle [3] has been reported to vary with other types of damage [32] such as mechanical polishing. Broadening of the G and D peaks has been reported in Raman spectra obtained for a graphite block that had been exposed to the edge plasma produced in the TEXTOR tokamak (Tokamak Experiment for Technology Oriented Research) at around 300 to 400°C [53].

In this work, the D_1 peak will be referred to as simply the D peak, and the D_1/G peak ratio will be symbolized as I_D/I_G. Raman spectroscopy measurements were made on the Gilsocarbon and HOPG specimens and the neutron irradiated BEPO (Fig. 7) using a Renishaw Wire 522 nm UV laser source Raman Spectrometer. All measurements were repeated in triplicate. Reproducibility was very high, with a variation of less than 0.1% in peak intensity ratio.

The Raman spectra from fractured Gilsocarbon, Gilsocarbon dust and fractured BEPO were obtained on reflective facets, such as the depicted in Fig. 2, a7 and c1. In pristine HOPG

and on the facets of fractured Gilsocarbon, there is an almost complete absence of the D peak, (Fig. 7 b and i). BEPO, ion irradiated Gilsocarbon and ion irradiated HOPG present broadening of the D and G bands compared with non-irradiated HOPG Fig. 7, I) and all mechanically polished Gilsocarbon samples (Fig. 7, c to f). Mechanically polished Gilsocarbon produced very significant D peaks, whereas the Gilsocarbon dust (Fig. 7, a) clearly shows a low D band intensity.

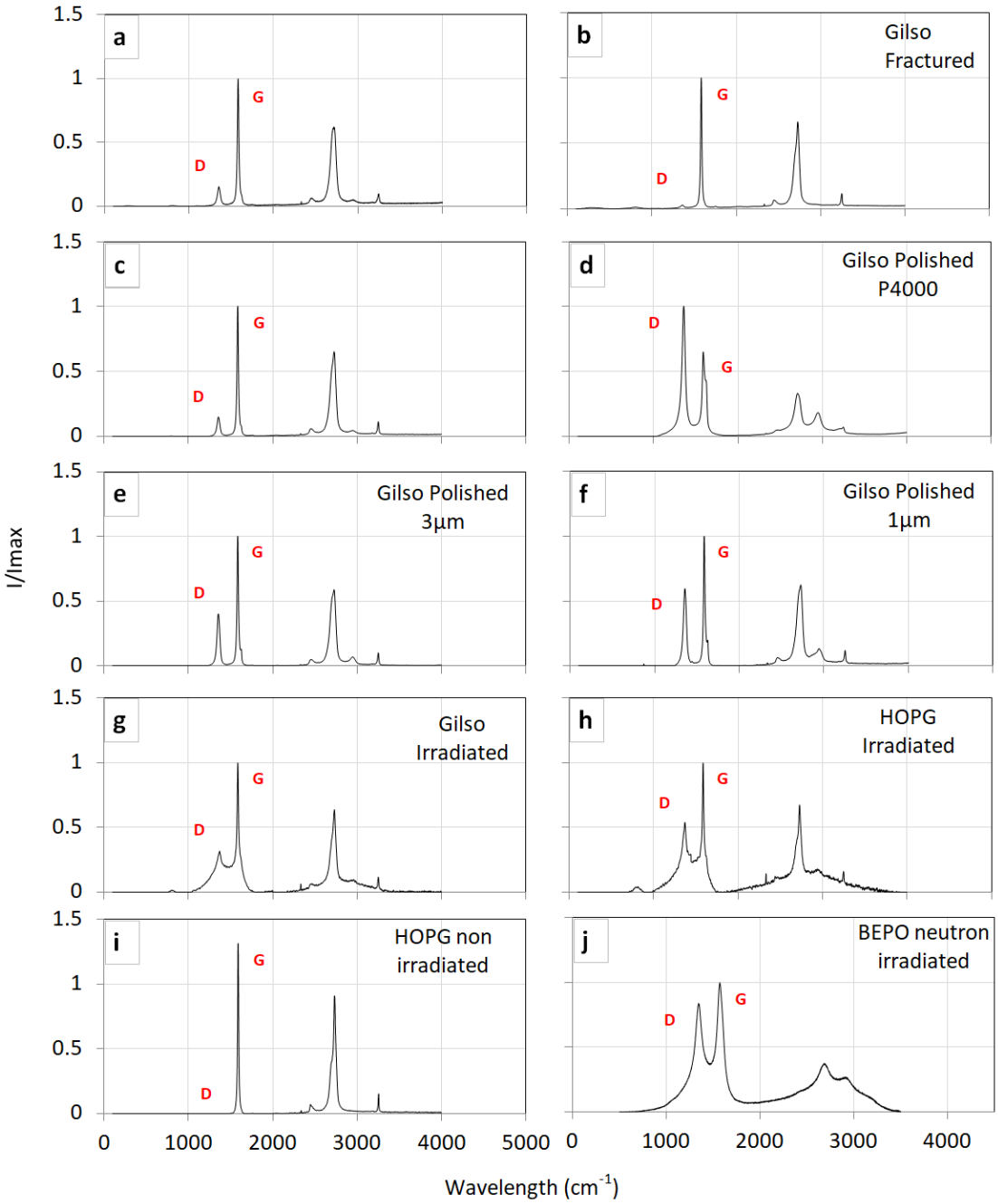

Fig. 7. A comparison between the Raman spectra of HOPG, and Gilsocarbon of various grades of polishing and fracturing to dust level

A calculation of the mean crystalline size between all the grades of surface treatment was done following the methodology of Tuinstra et al. [54], who found that in graphite the $I_{(D)}/I_{(G)}$ peak intensity ratio was inversely proportional to the mean crystalline size L_a:

$$\frac{I(D)}{I(G)} = \frac{C(\lambda)}{L_a}, \quad (2)$$

where C(λ) for a wavelength of 488 nm^{-1} is 4.4 nm [55-57]. The peaks attributed to the D band and G band (1340 and 1580cm^{-1} respectively) and the ratio of their intensities was used. The data are summarized in Table 3. This shows that the largest crystallite size was obtained for fractured non-irradiated Gilsocarbon (the cleaved HOPG has a negligible D-band). Crystallite dimensions of around 100 to 300 A are obtained for the majority of surfaces, with very fine size (~50 μm or less) for the neutron irradiated BEPO and finely ground Gilsocarbon.

Table 3. The calculated mean surface crystalline size, depending on the surface preparation method

	Polishing Particle Size	I_D/I_G (cm^{-1})	$\bar{L}_a$ (Angstroms)
Gilso Polished P800	21.8 μm	0.13	346.5
Gilso Polished P4000	5 μm	1.64	26.8
Gilso Polished 3μm	3μm	0.37	119.6
Gilso Polished 1μm	1μm	0.53	83.2
Gilso Ion Polished	-	0.25	174.6
BEPO Neutron Irradiated	-	0.82	53.6
HOPG Ion Polished	-	0.38	117.3
HOPG Pristine	-	0	∞
Gilso Dust	-	0.13	341.1
Gilso Fractured	-	0.01	2973

4. Discussion

Effect of the particle size. The effect of the particle size of the polishing paper was clearly evident from the resulting crystallinity values. SiC particles of polishing paper P4000 are about 2.5μm (median size), while for P800 they are 6.5 μm. Decreasing of mean polishing particle size, increased the D band and decreased the pseudo–crystallinity. Diamond paste polishing had a similar effect. A decrease of the mean particle size of the polishing paste from 3 μm to 1 μm, increased the D band and decreased the pseudo–crystallinity. In general, the least amount of damage was induced by fracturing techniques. The examination of Raman spectra showed that mechanical polishing produces large quantities of surface defects in Gilsocarbon.

Increase in fine porosity of Gilsocarbon. The increase in fine porosity of Gilsocarbon by ion beam polishing (Fig. 4) may be by opening of pro-existing covered pores when ion bombarded. The pores are uncovered by the abrasion of surface material during ion - bombardment. The facets and pores that are exposed during fracturing and ion beam polishing of Gilsocarbon are calcination cracks, produced due to the anisotropy of crystal thermal expansion and are thus deduced to be close to the basal plane. Fracturing exposes these pre-existing cracks. The Raman spectrum resemblance between fractured Gilsocarbon

with pristine HOPG reveals that very little proportion of natural damage exists in undisturbed polycrystalline graphite.

Crystalline size. The crystalline size that was calculated by Raman refers to the surface of the specimens [58]. Equation (2) calculated a statistical or two-dimension crystallinity. Although it cannot immediately provide information for the real crystalline size of the specimen, it can serve as an index of crystallinity to induced damage. It can characterize induced disorder during surface treatment. Only in the case of fractured Gilsocarbon, L may more specifically refer to the bulk crystallinity along the c axis. For pristine HOPG the crystallinity of the c axis is theoretically infinite since the D peak is absent.

Crystalline sizes calculated by Raman, do not totally agree with those calculated by XRD. This is expected since the penetration depth of X-rays is higher compared to most Raman laser beams. BEPO's mean crystalline size of 53.6 Angstroms (by Raman) is close to the 78.60 Angstroms (by XRD). Various crystalline sizes were calculated for all the specimens of Gilsocarbon for all degrees of mechanical polishing.

The crystallite sizes calculated are consistent with literature data; in the range of 300 Å [59]. However, the crystallite dimensions reported using Raman spectra cannot necessarily be regarded as real crystallites. They are indicative statistical parameters that serve as an index of the degree of microstructural order. The same applies to HOPG, the structure of which resembles that of a mono-crystal with no distinct grain boundaries. The crystallinity of BEPO is decreased compared to the other graphites due to the increase of disorder from neutron irradiation. Ion beam polishing affects the microstructure of Gilsocarbon to a certain depth, traceable by XRD. Its crystallinity decreased by 40 to 50 Angstroms after irradiation (Table 3). This was despite the fact that ion irradiation took place on the surface and neutron irradiation happened throughout the graphite mass. In addition, irradiation did not change the crystalline sizes of HOPG (Table 2).

Ion bombardment. Ion irradiated HOPG forms pits that originate from corrugations formed while the specimen was being ion polished (Fig. 4 b, e, Fig. 5, b). Irradiation disrupted the original "mirror" surface of HOPG and produced formations resembling fish scales. The surface area ratio increases for HOPG and decreases for Gilsocarbon after ion irradiation. A similar increase of surface roughness in HOPG, which is consistent with the observed corrugations of most of the basal flat surfaces, occurs. Ion irradiation decreases surface roughness in Gilsocarbon. The corrugations in HOPG have the form of a network (Fig. 4 b, e, Fig. 5, b) which suggests that defects, produced during ion bombardment, move and agglomerate to form a network. During the bombardment, the defects migrate and agglomerate, producing territories of prismatic and basal dislocations [60]. Kelly et al. [61] summarized the various defect categories, as well as their formation mechanisms. The observed structures (Fig. 4 b, e, Fig. 5, b) could be considered as pseudo-crystallite boundaries perpendicular to the basal planes, thereby defining a pseudo-crystallite size L_a. Moving vacancies can be trapped within these boundary territories. These corrugations may also be collapsed lines of vacancies which contract the basal planes. It has been proven that they do not absorb diffusing interstitial atoms [62,63].

The above observations support the findings of Kitajima et al. [64] and Asari et al. [65,66] who claimed that defects are distributed among the c-planes and interstitial atoms displaced by bombardment do not come to rest between them. Therefore during the bombardment of HOPG, the ion flux is directly affecting the c planes. Thus, the produced vacancies and interstitials are distributed along the *c*-planes and less likely to reside between them. In this manner, the "*c* crystallinity" is not affected. The same does not apply for polycrystalline graphite such as Gilsocarbon, comprising of crystallites with arbitrary orientation with respect to the ion beam.

5. Conclusions

The smoothest surfaces are achieved in pristine HOPG by cleaving, followed by fractured Gilsocarbon surfaces and Gilsocarbon surfaces produced by ion beam irradiation. Mechanical polishing with P4000 of Gilsocarbon followed. The diamond paste produced rougher surfaces than P4000. A decrease of the mean particle size of the polishing paste from 3 μm to 1 μm and even the use of smaller particles such as ions and neutrons increased the D band and decreased the pseudo–crystallinity. In general, the decrease of the particle size of the polishing agent increased the microstructural damage. The effect of the particle size of the polishing agent was clearly evident from the resulting Raman pseudo-crystallinity values. The Raman spectrum resemblance between fractured Gilsocarbon with pristine HOPG reveals that very little micro-damage exists in undisturbed graphitic specimens. The produced vacancies and interstitials are distributed along the c-planes and less likely between them. Based on the findings of this work, it is recommended that preferably fracture of specimens to take place at microstructural studies on graphite, rather than other more damaging sample preparation methods.

Acknowledgements. *The authors would like to acknowledge financial assistance to the Greek State Scholarships Foundation. He would also like to acknowledge substantial laboratory assistance to Serco Assurance – Warrington – Risley, UK (Now Wood PLC), as well as the Materials Performance Center, School of Materials, University of Manchester for financial support. They would also like to thank the United Kingdom Atomic Energy Authority (UKAEA), with permission from the Nuclear Decommissioning Authority (NDA) for provision of radioactive graphite samples. Professors Abbie Jones, and Paul Mummery, of the Nuclear Graphite Research Group are kindly acknowledged for their assistance in handling of radioactive materials.*

References

[1] Preston S. *Preliminary measurements of stored energy in graphite dowels from the Windscale piles*. AEA Technology. Industrial report, 1997.
[2] Simmons J. *Stored energy In the Windscale Piles*. AEA Technology. Report number: AEA RS 5283, 1994.
[3] Iwata T. Fine structure of Wigner energy release spectrum in neutron irradiated graphite. *Journal of Nuclear Materials*. 1985;133-134: 361-364.
[4] Nightingale RE, Davidson JM, Snyder WA. *Damage effects to graphite irradiated up to 1000 C*. General Electric Co. Hanford Atomic Products Operation. Report number: NSA-12-014636, 1958.
[5] Marsden B. *Modelling Stored Energy Release*. The University of Manchester. Report number: NGRG R 139, 2004.
[6] Kelly BT, Marsden BJ, Hall K, Martin DG, Harper A. *Irradiation damage in graphite due to fast neutrons in fission and fusion systems*. Vienna: IAEA; 2000.
[7] Tsang DKL, Marsden BJ, Fok SL, Hall G. Graphite thermal expansion relationship for different temperature ranges. *Carbon.* 2005;43(14): 2902-2906.
[8] Burchell TD, Murty KL, Eapen J. Irradiation induced creep of graphite. *Materials for Nuclear Power*. 2010;62(9): 93-99.
[9] Kelly BT. Irradiation creep in graphite—some new considerations and observations. *Carbon*. 1992;30(3): 379-383.
[10] Tsang DKL, Marsden BJ, Vreeling JA, van der Laan J. Analyses of a restrained growth graphite irradiation creep experiment. *Nuclear Engineering and Design*. 2008;238(11): 3026-3030.

[11] Snead LL, Burchell TD, Katoh Y. Swelling of nuclear graphite and high quality carbon fiber composite under very high irradiation temperature. *Journal of Nuclear Materials.* 2008;381(1–2): 55-61.
[12] Marsden B, Hall G, Woutersb O, Vreeling J, van der Laan J. Dimensional and material property changes to irradiated Gilsocarbon graphite irradiated between 650 and 750°C. *Journal of Nuclear Materials.* 2008;381(1-2): 62-67.
[13] Smith DJ. Characterisation of Nanomaterials Using Transmission Electron Microscopy. In: Kirkland AI, Haigh SJ. (eds.) *Nanocharacterisation*. 2nd ed. Arizona State University; 2015. p.1-29.
[14] Mitra S. *Sample Preparation Techniques in Analytical Chemistry*. Hoboken, New Jersey: John Wiley & Sons, Inc.; 2003.
[15] Ma L. Comparison of different sample preparation techniques in TEM observation of microstructure of INCONEL alloy 783 subjected to prolonged isothermal exposure. *Micron.* 2004;35(4): 273-279.
[16] Fiawoo M, Bonnot A, Jourdain V, Michel V, Picher M, Arenal R, Thibault-Pénisson J, Loiseau A. Substrate preparation techniques for direct investigation by TEM of single wall carbon nanotubes grown by chemical vapor deposition. *Surface Science.* 2009;603(8): 1115-1120.
[17] Rubanov S, Suvorova A. The Study of the FIB Induced Damage in Diamond. *Microscopy and Microanalysis*. 2011;17(52): 700-701.
[18] Ammar M, Rouzaud J, Vaudey C, Toulhoat N, Moncoffre N. Characterization of graphite implanted with chlorine ions using combined Raman microspectrometry and transmission electron microscopy on thin sections prepared by focused ion beam. *Carbon.* 2010;48(4): 1244-1251.
[19] Ishioka K, Hase M, Ushida K, Kitajima M. Coherent acoustic phonon-defect scattering in graphite. *Physica B: Condensed Matter*. 2002;316-317: 296-299.
[20] Liu J, Hou MD, Trautmann M, Neumann CR, Muller C, Wang ZG, Zhang QX, Sun YM, Jin YF, Liu HW, Gao HJ. STM and Raman spectroscopic study of graphite irradiated by heavy ions. *Nuclear Instruments and Methods in Physics Research Section B: Beam Interactions with Materials and Atoms*. 2003;212: 303-307.
[21] Niwase K. Formation of dislocation dipoles in irradiated graphite. *Materials Science and Engineering – A.* 2005;400-401: 101-104.
[22] Hida A, Meguro T, Maeda K, Aoyagi Y. Analysis of surface modifications on graphite induced by slow highly charged ion impact. *Nuclear Instruments and Methods in Physics Research Section B: Beam Interactions with Materials and Atoms*. 2003;205: 736-740.
[23] Hinks JA, Haigh SJ,Greaves G, Sweeney F, Pan CT, Young RJ, Donnelly SE. Dynamic microstructural evolution of graphite under displacing irradiation. *Carbon.* 2014;68: 273-284.
[24] Mostafavi M, McDonald. S, Çetinel H, Mummery P, Marrow T. Flexural strength and defect behaviour of polygranular graphite under different states of stress. *Carbon.* 2013;59: 325-336.
[25] Preston S, Marsden B. Changes in the coefficient of thermal expansion in stressed Gilsocarbon graphite. *Carbon.* 2006;44(7): 1250-1257.
[26] Yang C, Lu Y, Hwang I. Imaging surface nanobubbles at graphite–water interfaces with different atomic force microscopy modes. *Journal of Physics: Condensed Matter.* 2013;25(18): 184010.
[27] Ferreira Q, Braganc A, Moura N, Faustino M, Alcácer L, Morgado J. Dynamics of porphyrin adsorption on highly oriented pyrolytic graphite monitored by scanning tunnelling microscopy at the liquid/solid interface. *Applied Surface Science* 2013:273: 220-225.

[28] Krishna R, Jones A, Mcdermott L, Marsden B. Irradiation Damage Studies in BEPO Graphite using High Resolution Transmission Electron Microscopy and Raman Spectroscopy. *MRS Online Proceedings*. 2012;1475: 1-19.
[29] Gallego N C. Burchell TD. *A Review of Stored Energy Release of Irradiated Graphite*. U.S. Department of Energy . Report number: ORNL/TM-2011/378, 2011.
[30] Lasithiotakis M, Marsden BJ, Marrow TJ. Application of an independent parallel reactions model on the annealing kinetics of BEPO irradiated graphite. *Journal of Nuclear Materials*. 2012:427(1-3): 95-109.
[31] Ziegler JF, Ziegler MD, Biersack JP. SRIM - the stopping and range of ions in matter. *Nuclear Instruments and Methods in Physics Research Section B: Beam Interactions with Materials and Atoms*. 2010;268: 1818-1823.
[32] International Standard. ISO 1302:2002(E). *Geometrical Product Specifications (GPS) - Indication of surface texture in technical product documentation.* Geneva; ISO; 2002.
[33] International Standard. ISO 4287:1997(E/F). *Geometrical Product Specifications (GPS) - Surface texture: Profile method - Terms, definitions and surface texture parameters.* Geneva; ISO; 1997.
[34] International Standard. ISO 4287-1:1984. *Surface roughness -- Terminology -- Part 1: Surface and its parameters*. Geneva; ISO; 1984.
[35] An American National Standard. ASME B46.1-2009. *Surface Texture (Surface Roughness, Waviness, and Lay).* US: ASME; 2020.
[36] Meguro T, Hida A, Koguchi Y, Miyamoto S, Yamamoto Y, Takai H, Maeda K, Aoyagi Y. Nanoscale transformation of sp2 to sp3 of graphite by slow highly charged ion irradiation. *Nuclear Instruments and Methods in Physics Research Section B: Beam Interactions with Materials and Atoms* 2003;209: 170-174.
[37] Smith R, Smith G, Weightman P. Effects of low energy argon ion irradiation on the carbon 1s photoelectron line of highly oriented pyrolytic graphite. *Journal of Electron Spectroscopy and Related Phenomena*. 2006;152(3): 152-157.
[38] Franklin R. The structure of graphitic carbons. *Acta Crystallographica.* 1951;4: 253-261.
[39] Howe JY, Rawn CJ, Jones LE, Ow H. Improved crystallographic data for graphite. *Powder Diffraction*. 2003;18(2): 150-154.
[40] Kelly B. Radiation Damage in Graphite and its Relevance to Reactor Design. *Progress in Nuclear Energy*. 1978;2(4): 257-269.
[41] Zhou Z, Bouwman WG, Schut H, Pappas C. Interpretation of X-ray diffraction patterns of (nuclear) graphite. *Carbon.* 2014;69: 17-24.
[42] Lexa D. An improved hermetic sample enclosure for simultaneous differential scanning calorimetry/synchrotron powder X-ray diffraction. *Thermochimica Acta.* 2003;398(1-2): 241-248.
[43] Chi S, Kim G. Comparison of 3 MeV C+ ion-irradiation effects between the nuclear graphites made of pitch and petroleum cokes. *Journal of Nuclear Materials.* 2008;381(1-2): 98-105.
[44] Li Z. Characterization of Different Shaped Nanocrystallites using X-ray Diffraction Line Profiles. *Particle & Particle Systems Characterization*. 2011;28(1-2): 19-24.
[45] Black G, Marsden B, Wright G, Jones A. Origin and validity of graphite dosimetry units and related conversion factors. *Annals of Nuclear Energy.* 2016;94: 241-250.
[46] Liu J, Yao HJ, Sun YM, Duan JL, Hou MD, Mo D, Wang ZG, Jin YF, Abe H, Li ZC, Sekimura N. Temperature annealing of tracks induced by ion irradiation of graphite. *Nuclear Instruments and Methods in Physics Research B.* 2006;245(1): 126-129.
[47] Asari E. An effect of the extended cascade on the Raman spectra of ion-irradiated graphite. *Carbon*. 2000;38(13): 1857-1861.

[48] Compagnini G, Puglisi O, Foti G. Raman spectra of virgin and damaged graphite edge planes. *Carbon*. 1997;35(12): 1793-1797.
[49] Ferrari A, Robertson C. Interpretation of Raman spectra of disordered and amorphous carbon. *Physical Review B*. 2000;61(20): 14095-14107.
[50] Nakamizo M, Tamai K. Raman spectra of the oxidized and polished surfaces of carbon. *Carbon.* 1984;22(2): 197-198.
[51] Manika I, Maniks J, Zabels R, Gabrusenoks J, Krause M, Tomut M, Schwartz K. Nanoindentation and Raman Spectroscopic Study of Graphite Irradiated with Swift 238U Ions. *Fullerenes, Nanotubes and Carbon Nanostructures*. 2012;20(4-7): 548-552.
[52] Niwase K. Formation of dislocation dipoles in irradiated graphite. *Materials Science and Engineering A*. 2005;400-401(1-2 SUPPL.): 101-104.
[53] Hirai T, Compan J, Niwase K, Linke J. Laser Raman microprobe analysis of graphite exposed to edge plasma in the TEXTOR tokamak. *Journal of Nuclear Materials*. 2008;373(1-3): 119-127.
[54] Tuinstra F, Koenig J. Raman Spectrum of Graphite. *Journal of Chemical Physics*. 1970;53(3): 1126-1130.
[55] Knight D, White W. Characterization of diamond films by Raman spectroscopy. *Journal of Materials Research*. 1989;4(2): 385-394.
[56] Sinha K, Menendez J. Resonant First- and Second-Order Raman Scattering in Graphite. *Physical Review B.* 1990;41(15): 10845-10847.
[57] Matthews M, Pimenta M, Dresselhaus G, Dresselhaus M, Endo M. Origin of dispersive effects of the Raman D band in carbon materials. *Physical Review B.* 1999;59(10): R6585-R6588.
[58] Asari E. An effect of the extended cascade on the Raman spectra of ion-irradiated graphite. *Carbon*. 2000;38(13): 1857-1861.
[59] Simmons J. *Stored Energy in the Windscale Piles.* AEA Technology. Report number: 5283, 1994.
[60] Telling R, Heggie M. Radiation Damage in Graphite. *Philosophical Magazine.* 2007;87(31): 4796-4846.
[61] Kelly BT. The theory of irradiation damage in graphite. *Carbon.* 1977;15(2): 117-129.
[62] Lidiard AB, Perrin R. The growth of interstitial clusters in graphite under irradiation. *The Philosophical Magazine: A Journal of Theoretical Experimental and Applied Physics*. 1966;14(129): 433-444.
[63] Kelly T, Mark W, Price A, Bland J. The mechanism of dimensional changes in the crystals of graphites and carbons under fast neutron irradiation. *The Philosophical Magazine: A Journal of Theoretical Experimental and Applied Physics.* 1966;14(128): 343-356.
[64] Asari E, Nakamura KG, Kawabe T, Kitajima M. Observation of relaxation processes of disorder in ion-irradiated graphite using Raman spectroscopy. *Journal of Nuclear Materials.* 1997;244(2): 173-175.
[65] Asari E, Kitajima M, Nakamura KG, Kawabe T. Thermal relaxation of ion irradiated damage in graphite. *Physical Review B: Condensed Matter and Materials Physics*. 1993;47(17): 11143-11148.
[66] Asari E, Kamioka I, Lewis WA, Kawabe TI, Nakamura KG, Kitajima M. Ion mass effect on lattice disordering rate of graphite under low energy ion irradiation. *Nuclear Instruments and Methods in Physics Research Section B: Beam Interactions with Materials and Atoms.* 1994;91(1-4): 545-548.